

# Pictorial Representation of Anisotropy and Macroscopic Reorientations of Samples in Solid-State NMR: First-Order Interactions

C. Bonhomme\* and J. Livage

Laboratoire de Chimie de la Matière Condensée, URA CNRS 1466, Université Pierre et Marie Curie, 4 Place Jussieu, 75252 Paris, Cedex 05, France

Received: August 1, 1997; In Final Form: November 3, 1997<sup>⊗</sup>

In solid-state NMR, spectra of powdered samples are dominated by the anisotropy of the involved interactions. All internal interactions can be described by second-rank tensors, which account for the observed broadening of the lines. A well-known representation of these tensorial effects is the so-called “representation ellipsoid”. It allows a direct pictorial representation of any first-order interaction. However, an ellipsoid can be defined only for strictly positive principal components of a given tensor. More complicated surfaces, such as ovaloids, were introduced recently for the direct representation of tensorial properties and for every set of principal components. In this paper, we show that the “representation ellipsoid” can be extended to generalized quadrics (including cylinders, hyperboloids, and degenerate surfaces), avoiding the use of ovaloids. Moreover, such quadrics can be used for a very simple representation of macroscopic reorientation techniques of samples such as magic-angle spinning, variable-angle spinning, and switching-angle spinning, as well as for the description of rapid anisotropic molecular motions. No explicit reference to Legendre polynomials was made. This article is the first step for a Cartesian representation of higher-order NMR interactions and higher-order macroscopic trajectories such as dynamic-angle spinning, double-rotation, or multiple-quantum magic-angle spinning.

## 1. Introduction

In the presence of a large external static field  $B_0$ , solid-state NMR spectra of powders are usually characterized by broad, featureless lines even in the case of simple systems involving one or few crystallographic sites. Indeed, all internal interactions that are present at a given nucleus (such as chemical shielding, homo- and/or heteronuclear dipolar coupling, quadrupolar interaction) can be described by second-rank tensors.<sup>1</sup> It follows that the spin interactions depend on the orientation of  $B_0$  relative to each principal axes system (see below) related to the nucleus of interest; therefore, frequency dispersion is observed. In the case of powdered samples (involving for instance one unique crystallographic site), integration over the crystallite's orientation distribution<sup>2</sup> leads to the well-known “powder patterns”, characteristic for the various spin interactions: chemical shift anisotropy (CSA),<sup>3</sup> Pake doublet<sup>4</sup> for dipolar coupling or first-order quadrupolar interaction for spin  $I = 1$ , central transition and satellites patterns<sup>5</sup> for  $I = n/2$  ( $n = 3, 5, 7, 9$ ), central transition broadened by second-order quadrupolar interaction,<sup>6</sup> and so forth. Several interactions of the same order of magnitude may be present, leading to complex line shapes. The resolution is definitively lost when several broad lines overlap. Several pictorial representations of tensors have been given in the literature, accounting at least for first-order effects of the different NMR interactions. The most popular representation is the so-called “representation ellipsoid”.<sup>1,7</sup> This approach is essentially Cartesian (involving  $3 \times 3$  matrices) and has been applied to many symmetrical second-rank physical properties.<sup>7</sup> It can be shown that the intersection of this ellipsoid in the  $B_0$  direction is directly related to the magnitude of any first-order perturbation. As the

orientation of  $B_0$  from the ellipsoid axes varies from one crystallite to another in a powder sample, a direct representation of the interaction anisotropy is obtained. However, the “representation ellipsoid” implies that the three semiaxes can be defined. In other words, the three principal components of the given tensor must be strictly positive. Recently, several authors have developed a different pictorial representation based on ovaloids.<sup>8,9</sup> This representation holds for every set of principal components, including zero and/or negative principal components. In this article, we show that the use of ovaloids (which correspond to sixth-degree surfaces) is not necessary. The “representation ellipsoid” can be easily extended to generalized quadrics (second-degree surfaces, including degenerate cases), accounting for every set of principal components. Emphasis will be made on traceless tensors, related for instance to dipolar or quadrupolar interactions. Generalized quadrics will also be used for the pictorial representation of fast molecular reorientations (and their effects on anisotropies) and two-dimensional correlations between interactions.

To retrieve resolution in a solid-state NMR experiment, spatial anisotropies must be removed. In the case of an isotropic liquid, rapid and random molecular reorientation eliminates anisotropic spectral broadening. Narrow lines are obtained, and only the isotropic components of the spin interactions (related to the traces of the involved tensors) are thus measured. In solid-state NMR, high-resolution spectra can be obtained by either averaging in spin space<sup>2</sup> and/or averaging in real space. In this work, we shall focus on averaging in real space. As shown first by Andrew<sup>10</sup> and Lowe,<sup>11</sup> rapid reorientation of a powder sample around the “magic-angle”  $\theta = \zeta_m = 54.74^\circ$  or magic-angle spinning (MAS) can remove anisotropies related to first-order interactions. MAS is a routine technique of solid-state NMR. The mathematical treatment of this averaging procedure

<sup>⊗</sup> Abstract published in *Advance ACS Abstracts*, December 15, 1997.

is based on the general transformation properties of second-rank tensors under rotation, including the irreducible spherical representation of tensors, Wigner rotation matrices, and the second-order Legendre polynomial  $P_2(\cos \theta)$  ( $\theta$  corresponds to the angle between the rotor axis and  $B_0$ ).<sup>1,2</sup> This approach was extended recently to the effect of macroscopic reorientation on line shapes broadened by second-order interactions (such as second-order quadrupolar interaction). In this case, it is now well-known that rapid MAS cannot completely eliminate anisotropic broadening effects.<sup>12</sup> The ingenious derivation of Hamiltonians in terms of second- and fourth-order Legendre polynomials  $P_2(\cos \theta)$  and  $P_4(\cos \theta)$  led to the conception of new experimental schemes such as dynamic-angle spinning (DAS), double-rotation (DOR),<sup>13–15</sup> and multiple-quantum magic-angle spinning (MQ-MAS),<sup>16</sup> allowing the total suppression of second-order effects. More generally, MAS, DAS, and DOR trajectories have been analyzed in terms of symmetry imposed to the sample under reorientation.<sup>17</sup> In this paper, we give a pictorial representation of MAS (for first-order interactions), taking advantage of the generalized quadrics cited above. Spherical tensors, which are extensively used as far as solid-state NMR is concerned, are not used in this work. Explicit reference to  $P_2(\cos \theta)$  will not be made. A pictorial representation of magic-angle hopping (MAH)<sup>18</sup> and variable-angle spinning (VAS)<sup>19</sup> will be presented as well. It will also be shown that the generalized quadrics are not suitable for the representation of second-order effects on the line shapes. This article is the first step for the direct Cartesian representation of second-order effects by fourth-degree surfaces. It will be shown that the effects of MAS, VAS, and higher-order trajectories on quadrupolar nuclei can be easily understood by considering these novel surfaces and simple Cartesian frame transformations. Once again, explicit reference to  $P_2(\cos \theta)$  and  $P_4(\cos \theta)$  will not be necessary.

In this paper, the following plan is adopted: section 2 is devoted to the direct pictorial representation of first-order NMR interactions by quadrics. This section gives general rules for the representation. Applications of this representation to the effect of molecular reorientation and to 2D correlations in static NMR experiments are presented in section 3. The description of the effects of MAS, MAH, and VAS are given in sections 4, 5, and 6, respectively. Finally, the reorientation of samples around two axes (for  $I = 1/2$ ) and higher-order interactions are described in section 7.

## 2. Representation of First-Order Interactions

In the presence of a strong external magnetic field  $B_0$ , the relevant Hamiltonian  $\hat{H}$  related to the nucleus of interest can be written as  $\hat{H} = \hat{H}_{\text{ext}} + \hat{H}_{\text{int}}$ , where<sup>1,20</sup>

$$\begin{aligned} \hat{H}_{\text{ext}} &= \hat{H}_Z + \hat{H}_{\text{RF}} \\ \hat{H}_{\text{int}} &= \hat{H}_\sigma + \hat{H}_D + \hat{H}_Q + \hat{H}_J + \hat{H}_{\text{SR}} \end{aligned} \quad (2.1)$$

The external interactions correspond to the Zeeman ( $\hat{H}_Z$ ) and radiofrequency ( $\hat{H}_{\text{RF}}$ ) Hamiltonians. The different terms in  $\hat{H}_{\text{int}}$  correspond to the shielding interaction ( $\hat{H}_\sigma$ ), homo- and heteronuclear dipolar coupling ( $\hat{H}_D$ ), quadrupolar interaction ( $\hat{H}_Q$  if  $I > 1/2$ ), indirect coupling ( $\hat{H}_J$ ), and spin-rotation interaction ( $\hat{H}_{\text{SR}}$ ). In this paper, we focus on  $\hat{H}_\sigma$ ,  $\hat{H}_D$ , and  $\hat{H}_Q$ , as they represent the most important NMR interactions. However, the results derived for these three interactions may be extended to the others. All internal interactions  $\hat{h}^{-1}\hat{H}_{\text{int}}$  (in angular velocity units) may be represented by second-rank tensors  $[\mathbf{T}]$  such that

$\hat{h}^{-1}\hat{H}_{\text{int}} = k_{\text{T}}\hat{I}[\mathbf{T}]Y_{\text{T}}$ , following the notations given by Harris.<sup>20</sup> The spin  $\hat{I}$  corresponds to the nucleus of interest;  $Y_{\text{T}}$  is another vector quantity. For  $[\mathbf{T}] = [\boldsymbol{\sigma}]$ ,  $Y_{\text{T}} = B_0$ . For  $[\mathbf{T}] = [\mathbf{D}]$ ,  $Y_{\text{T}} = S$  (a spin different from  $I$ , accounting for homo- and heteronuclear dipolar coupling). For  $[\mathbf{T}] = [\mathbf{q}]$ ,  $Y_{\text{T}} = I$ . The parameter  $k_{\text{T}}$  adjusts the magnitude and dimension of the  $[\mathbf{T}]$  tensor. We suppose that  $[\mathbf{T}]$  is a symmetrical tensor, and we neglect therefore antisymmetric contributions.<sup>2</sup> For each tensor  $[\mathbf{T}]$ , one can choose a particular axes system (XYZ) or principal axes system (PAS) in which  $[\mathbf{T}]$  is diagonal.  $T_{XX}$ ,  $T_{YY}$ , and  $T_{ZZ}$  are the principal components. When considering  $[\mathbf{T}]_{\text{PAS}}$  and the principal components, other quantities can be defined:

$$\text{the isotropic component: } T_{\text{iso}} = (T_{XX} + T_{YY} + T_{ZZ})/3 \quad (2.2)$$

the anisotropy: two alternative definitions are generally proposed in the literature

$$\Delta T = T_{ZZ} - (T_{XX} + T_{YY})/2 \quad (2.3a)$$

$$(\delta_{\text{A}})_{\text{T}} = T_{ZZ} - T_{\text{iso}} \quad (2.3b)$$

$$\text{the asymmetry: } \eta_{\text{T}} = \frac{T_{XX} - T_{YY}}{T_{ZZ} - T_{\text{iso}}} \quad (0 \leq \eta_{\text{T}} \leq 1) \quad (2.4)$$

using the convention:

$$|T_{ZZ} - T_{\text{iso}}| \geq |T_{YY} - T_{\text{iso}}| \geq |T_{XX} - T_{\text{iso}}| \quad (2.5)$$

Other conventions may be found in the literature. The different PAS are not necessarily coincident. In the respective PASs

$$k_{\sigma}[\boldsymbol{\sigma}] = \gamma_{\text{I}} \begin{bmatrix} \sigma_{XX} & 0 & 0 \\ 0 & \sigma_{YY} & 0 \\ 0 & 0 & \sigma_{ZZ} \end{bmatrix} \quad (2.6)$$

$$k_{\text{D}}[\mathbf{D}] = 2\pi D \begin{bmatrix} 1 & 0 & 0 \\ 0 & 1 & 0 \\ 0 & 0 & -2 \end{bmatrix} \quad (2.7a)$$

$$D = \frac{\mu_0}{4\pi} \frac{\hbar}{2\pi} \frac{\gamma_{\text{I}}\gamma_{\text{S}}}{r_{\text{I-S}}^3} \quad (2.7b)$$

$$k_{\text{Q}}[\mathbf{q}] = \frac{e^2 Q}{2I(2I-1)\hbar} \begin{bmatrix} q_{XX} & 0 & 0 \\ 0 & q_{YY} & 0 \\ 0 & 0 & q_{ZZ} \end{bmatrix} \quad (2.8)$$

$r_{\text{I-S}}$  corresponds to the internuclear distance. The tensor  $[\mathbf{D}]$  is axially symmetric ( $\eta_{\text{D}} = 0$ ) and traceless.  $Q$  corresponds to the quadrupole moment of the nucleus. For  $i = X, Y$ , and  $Z$ ,  $eq_{ii} = V_{ii}$  and  $V_{ii}$  are the Cartesian components of the electric field gradient (EFG). This tensor is not necessarily axially symmetric ( $\eta_{\text{Q}}$  may be different from zero) but is traceless (in agreement with the Laplace equation, that is  $\sum_{X,Y,Z} q_{ii} = 0$ ).

To estimate the effects of anisotropy on the line shapes, the diagonal tensor  $[\mathbf{T}]_{\text{PAS}}$  must be expressed in the laboratory (LAB) frame ( $X_0Y_0Z_0$ ) where the  $B_0$  direction and  $Z_0$  are coincident. The LAB frame is derived from the PAS frame by the Euler angles ( $\alpha_0, \beta_0, \gamma_0$ ) which are given in Figure 1. The expression of  $[\mathbf{T}]$  in the LAB frame is then given by

$$[\mathbf{T}]_{(X_0Y_0Z_0)} = P^{-1}(\alpha_0, \beta_0, \gamma_0) \begin{bmatrix} T_{XX} & 0 & 0 \\ 0 & T_{YY} & 0 \\ 0 & 0 & T_{ZZ} \end{bmatrix}_{(PAS)} P(\alpha_0, \beta_0, \gamma_0) \quad (2.9)$$

$P$  is given in the Appendix. Moreover,  $P^{-1} = {}^tP$ . When dealing with secular parts of the different Hamiltonians and restricting ourselves to first-order perturbation effects, only the term  $T_{Z_0Z_0}$  in  $[\mathbf{T}]_{(X_0Y_0Z_0)}$  is relevant. Using eq 2.9,

$$T_{Z_0Z_0} = \cos^2 \alpha_0 \sin^2 \beta_0 T_{XX} + \sin^2 \alpha_0 \sin^2 \beta_0 T_{YY} + \cos^2 \beta_0 T_{ZZ} \quad (2.10)$$

In a powder sample,  $T_{Z_0Z_0}$  represents the magnitude of the tensor  $[\mathbf{T}]$  for a particular crystallite. For this crystallite, the orientation of  $B_0$  in the PAS is given as in Figure 1. Using eqs 2.2–2.5 and 2.6–2.8, we deduce the NMR line positions of the spectrum for a given orientation of crystallite when considering the different interactions:

$$\text{shielding interaction: } \nu_\sigma = \frac{\gamma}{2\pi} B_0 (1 - \sigma_{Z_0Z_0}) \quad (2.11)$$

$\sigma_{Z_0Z_0}$  is given by eq 2.10 or

$$\sigma_{Z_0Z_0} = \sigma_{\text{iso}} + \frac{\Delta\sigma}{3} (3 \cos^2 \beta_0 - 1 + \eta_\sigma \sin^2 \beta_0 \cos 2\alpha_0) \quad (2.12a)$$

$$\sigma_{Z_0Z_0} = \sigma_{\text{iso}} + (\delta_A)_o \left[ \frac{1}{2} (3 \cos^2 \beta_0 - 1) + \frac{1}{2} \eta_\sigma \sin^2 \beta_0 \cos 2\alpha_0 \right] \quad (2.12b)$$

dipolar coupling: for an isolated heteronuclear  $I-S$  spin system, two  $I$  lines are observed at

$$\nu_D = \pm \frac{1}{2} D D_{Z_0Z_0} \quad (2.13)$$

$$D_{Z_0Z_0} = 1 - 3 \cos^2 \beta_0 \quad (2.14)$$

$D$  is given in eq 2.7b. In the case of homonuclear dipolar two-spin interaction

$$\nu_D = \pm \frac{3}{4} D D_{Z_0Z_0} \quad (2.15)$$

Again,  $D$  is given in eq 2.7b with  $\gamma_I = \gamma_S = \gamma$ .  $D_{Z_0Z_0}$  is given by eq 2.14.

quadrupolar interaction: the expression for a transition from  $m_1$  to  $m_1 - 1$  is given by

$$\nu_Q = \frac{3(1 - 2m_1)}{4I(2I - 1)} \frac{e^2 Q}{h} q_{Z_0Z_0} \quad (2.16)$$

Again,  $q_{Z_0Z_0}$  is given by eq 2.10 or

$$q_{Z_0Z_0} = \frac{1}{2} q_{ZZ} (3 \cos^2 \beta_0 - 1 + \eta_Q \sin^2 \beta_0 \cos 2\alpha_0) \quad (2.17)$$

$e^2 q_{ZZ} Q/h$  is the quadrupole coupling constant. For  $I = n/2$  ( $n = 3, 5, 7, 9$ ), the central transition ( $m_1 = 1/2$ ) is not shifted by the first-order quadrupolar interaction.  $m_1 \neq 1/2$  corresponds to the  $(2I - 1)$  satellites. For  $\eta_Q = 0$ ,

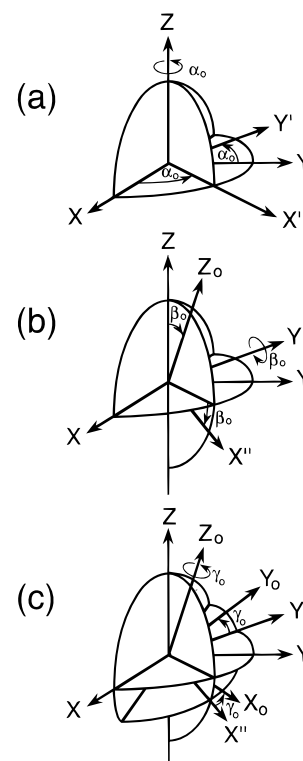


**Figure 1.** Definitions of the Euler angles  $(\alpha_0, \beta_0, \gamma_0)$  transforming a given PAS frame  $(XYZ)$  into the LAB frame  $(X_0Y_0Z_0)$ : (a) PAS frame is rotated counterclockwise around the  $Z$  axis by  $\alpha_0$ . This rotation generates a new frame  $(X'Y'Z)$ ; (b) counterclockwise rotation of the  $(X'Y'Z)$  frame around  $Y'$  by  $\beta_0$  generates a second intermediate frame  $(X''Y''Z)$ ; (c) this second intermediate frame is rotated counterclockwise by  $\gamma_0$  around  $Z_0$ , resulting in the  $(X_0Y_0Z_0)$  LAB frame. Using these definitions,  $\alpha_0$  and  $\beta_0$  represent the polar angles of the  $B_0$  direction in the PAS.

$$[\mathbf{q}] = -\frac{1}{2} q_{ZZ} \begin{bmatrix} 1 & 0 & 0 \\ 0 & 1 & 0 \\ 0 & 0 & -2 \end{bmatrix} \quad (2.18)$$

It is interesting to note that this tensor can be compared to  $[\mathbf{D}]$ , described by eq 2.7a.

As stated above, the role of  $T_{Z_0Z_0}$  is crucial. We shall now give a pictorial representation of this quantity. First, we restrict ourselves to strictly positive principal components; that is  $T_{ii} > 0$  ( $i = X, Y, Z$ ). In the PAS, we consider the quadric given by

$$T_{XX}X^2 + T_{YY}Y^2 + T_{ZZ}Z^2 = 1 \quad (2.19)$$

This quadric is an ellipsoid (Figure 2a), whose semiaxes are  $(T_{ii})^{-1/2}$ . When  $B_0$  is oriented from the PAS by the Euler angles  $(\alpha_0, \beta_0, \gamma_0)$  (Figure 1),  $B_0$  is located in the plane containing the  $X'$  ( $\alpha_0$ ) and  $Z$  axes. The intersection between this plane and the ellipsoid is an ellipse, whose equation in  $X'(\alpha_0)Z$  is

$$(\cos^2 \alpha_0 T_{XX} + \sin^2 \alpha_0 T_{YY})X'^2 + T_{ZZ}Z^2 = 1 \quad (2.20)$$

The radius  $r$  corresponding to the intersection of the ellipse with the  $B_0$  direction (Figure 2a) is then easily derived, using  $X' = r \sin \beta_0$ ,  $Z = r \cos \beta_0$ , and eq 2.20. One obtains

$$r = (\cos^2 \alpha_0 \sin^2 \beta_0 T_{XX} + \sin^2 \alpha_0 \sin^2 \beta_0 T_{YY} + \cos^2 \beta_0 T_{ZZ})^{-1/2} \quad (2.21a)$$

Using eq 2.10, it follows that

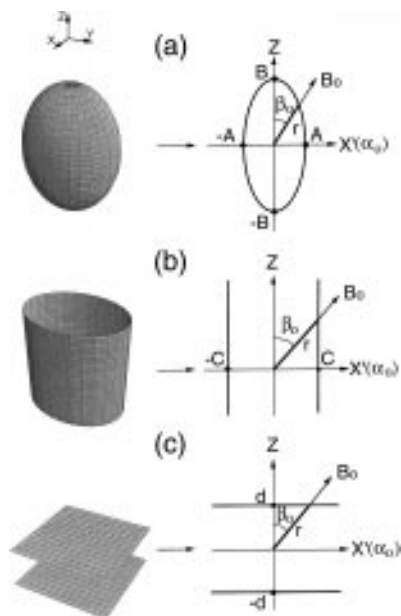


**Figure 2.** Pictorial representation of anisotropic first-order interactions for various  $\{T_{ii}\}$  sets. Intersections with the plane containing  $B_0$  and the  $X'(\alpha_0)$  and  $Z$  axes are also given. The  $(\alpha_0, \beta_0)$  angles are the polar angles of  $B_0$  and are referred to Figure 1. (a)  $T_{XX} > 0$ ,  $T_{YY} > 0$ , and  $T_{ZZ} > 0$  (ellipsoid).  $\mathbf{A} = (\cos^2 \alpha_0 T_{XX} + \sin^2 \alpha_0 T_{YY})^{-1/2}$ ;  $\mathbf{B} = (T_{ZZ})^{-1/2}$ . (b)  $T_{XX} > 0$ ,  $T_{YY} > 0$ , and  $T_{ZZ} = 0$  (elliptical cylinder).  $\mathbf{C} = (\cos^2 \alpha_0 T_{XX} + \sin^2 \alpha_0 T_{YY})^{-1/2}$ . (c)  $T_{XX} = T_{YY} = 0$ , and  $T_{ZZ} > 0$  (parallel planes).  $\mathbf{d} = (T_{ZZ})^{-1/2}$ .

$$1/r^2 = T_{Z_0Z_0} \quad (2.21b)$$

Equation 2.21b gives a simple geometrical representation of  $T_{Z_0Z_0}$ . It corresponds to the well-known “representation ellipsoid” related to symmetrical second-rank tensors, which is extensively used in crystal physics<sup>7</sup> or in solid-state NMR.<sup>1</sup> It can be noted that for  $\alpha_0 = 45^\circ$  and  $\beta_0 = \zeta_m$ ,  $r^{-2} = (T_{XX} + T_{YY} + T_{ZZ})/3 = T_{iso}$ . When  $[\mathbf{T}] = [\boldsymbol{\sigma}]$ ,  $\sigma_{iso}$  corresponds to the isotropic shielding at the nucleus, which may be observed in liquid-state NMR (neglecting solvent effects). Limitations of this representation are easily understood by considering the expressions of the semiaxes, that is  $(T_{ii})^{-1/2}$ . It imposes that  $T_{ii} > 0$ . For  $T_{ii} = 0$  and/or  $T_{ii} < 0$ , no real ellipsoid can be defined. Other surfaces can be used, such as ovaloids.<sup>8,9</sup> Ovaloids correspond to sixth-degree surfaces. In fact, the use of ovaloids is not necessary and generalized quadrics (second-degree surfaces) are suitable for the pictorial representation of  $T_{Z_0Z_0}$ . The expressions of these quadrics in the PAS are directly derived from eq 2.19. Three examples involving zero and negative principal components will now be given.

When  $T_{XX} > 0$ ,  $T_{YY} > 0$ , and  $T_{ZZ} = 0$ , eq 2.19 becomes (in the PAS)

$$T_{XX}X^2 + T_{YY}Y^2 = 1 \quad (2.22)$$

This equation corresponds to an elliptical cylinder (Figure 2b). The intersection of this cylinder by the  $X'(\alpha_0)Z$  plane corresponds to two parallel straight lines. Elementary geometry allows us to relate  $r$ ,  $\beta_0$ , and  $C$  (see Figure 2b) as  $\sin \beta_0 = C/r$ . It follows that  $r = (\cos^2 \alpha_0 \sin^2 \beta_0 T_{XX} + \sin^2 \alpha_0 \sin^2 \beta_0 T_{YY})^{-1/2}$ . Again,  $r^{-2} = T_{Z_0Z_0}$ , demonstrating the direct relation between these two quantities. One notes that  $\beta_0 \rightarrow 0$  leads to  $r \rightarrow \infty$ , as can be seen from Figure 2b, and  $T_{Z_0Z_0} \rightarrow 0$ . In other words, when  $B_0$  is parallel to the  $Z$  axis of the PAS, the  $T_{ZZ} (=0)$  principal component is attained. When  $\alpha_0 = 45^\circ$  and  $\beta_0 = \zeta_m$ ,  $r^{-2} = (T_{XX} + T_{YY})/3 = T_{iso}$ . In this particular case,  $T_{iso} > 0$ .

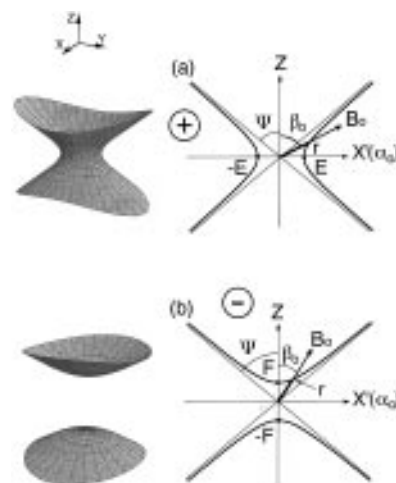


**Figure 3.** Pictorial representation of anisotropic first-order interactions for  $T_{XX} > 0$ ,  $T_{YY} > 0$ , and  $T_{ZZ} < 0$ . Intersections by the plane containing  $B_0$ , and the  $X'(\alpha_0)$  and  $Z$  axes are also given. (a) Elliptical hyperboloid of one sheet. When  $\beta_0 > \Psi(\alpha_0)$ , the equation  $+r^{-2} = T_{Z_0Z_0}$  holds. The sign of the first member of the equation is emphasized.  $\mathbf{E} = (\cos^2 \alpha_0 T_{XX} + \sin^2 \alpha_0 T_{YY})^{-1/2}$ ;  $tg^2 \Psi(\alpha_0) = |T_{ZZ}|/(\cos^2 \alpha_0 T_{XX} + \sin^2 \alpha_0 T_{YY})$ . (b) Elliptical hyperboloid of two sheets. When  $\beta_0 < \Psi(\alpha_0)$ , the equation  $-r^{-2} = T_{Z_0Z_0}$  holds. The sign of the first member of the equation is emphasized.  $\mathbf{F} = |T_{ZZ}|^{-1/2}$ .

When  $T_{XX} = T_{YY} = 0$  and  $T_{ZZ} > 0$ , eq 2.19 becomes (in the PAS)

$$T_{ZZ}Z^2 = 1 \quad (2.23)$$

The associated quadric is degenerate and corresponds to two parallel planes (Figure 2c). The intersection of these parallel planes by the  $X'(\alpha_0)Z$  plane corresponds to two parallel straight lines. Again, elementary geometry allows us to relate  $r$ ,  $\beta_0$ , and  $d$  (see Figure 2c), as  $\cos \beta_0 = d/r$ . It follows that  $r = (\cos^2 \beta_0 T_{ZZ})^{-1/2}$  or  $r^{-2} = T_{Z_0Z_0}$ . This expression is independent of  $\alpha_0$ , as the tensor is axially symmetric. When  $\beta_0 \rightarrow 90^\circ$ ,  $r \rightarrow \infty$  and  $T_{Z_0Z_0} \rightarrow 0$ . The zero principal components are attained.

When  $T_{XX} > 0$ ,  $T_{YY} > 0$ , and  $T_{ZZ} < 0$ , eq 2.19 becomes

$$T_{XX}X^2 + T_{YY}Y^2 - |T_{ZZ}|Z^2 = 1 \quad (2.24)$$



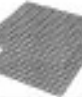



This situation is encountered in the case of the dipolar or quadrupolar interactions (see eqs 2.7a, 2.8, and 2.18). The following description is therefore particularly suitable for these interactions. Equation 2.24 corresponds to an elliptical hyperboloid of one sheet. One should note that this surface is not necessarily of revolution, as  $\eta_T$  may be different from zero (the case  $\eta_T = 0$  will be emphasized in section 3 and in Figure 5, when dealing with the heteronuclear dipolar interaction). The intersection of this hyperboloid by the  $X'(\alpha_0)Z$  plane corresponds to a hyperbola, whose equation in  $X'(\alpha_0)Z$  is

$$(\cos^2 \alpha_0 T_{XX} + \sin^2 \alpha_0 T_{YY})X^2 - |T_{ZZ}|Z^2 = 1 \quad (2.25)$$

This hyperbola exhibits two asymptotes, oriented from  $Z$  by  $\Psi(\alpha_0)$  (see Figure 3a). The expression of  $tg^2 \Psi(\alpha_0)$  can be easily derived, using  $X' = r \sin \beta_0$ ,  $Z = r \cos \beta_0$ , eq 2.25, and  $r \rightarrow \infty$ . It follows that

$$tg^2 \Psi(\alpha_0) = \frac{|T_{ZZ}|}{\cos^2 \alpha_0 T_{XX} + \sin^2 \alpha_0 T_{YY}} \quad (2.26)$$

Assuming that  $\beta_0 > \Psi(\alpha_0)$  and using eq 2.25, the intersection

$T_{XX}$	$T_{YY}$	$T_{ZZ}$	Quadric
+	+	+	<u>ellipsoid</u> 
+	+	0	<u>elliptical cylinder</u> 
0	0	+	<u>planes</u> 
0	0	0	<u>point</u> 
+	+	-	<u>elliptical hyperboloids</u> 
0	+	-	<u>hyperbolical cylinders</u> 

**Figure 4.** Generalized quadrics representing first-order interactions for every set  $\{T_{ii}\}$  of positive, negative, and zero principal components ( $i = X, Y, Z$ ).

radius  $r$  is then given by  $r^{-2} = \cos^2 \alpha_0 \sin^2 \beta_0 T_{XX} + \sin^2 \alpha_0 \sin^2 \beta_0 T_{YY} - \cos^2 \beta_0 |T_{ZZ}|$ . Comparing this expression and eq 2.10, it follows that  $+r^{-2} = T_{Z_0Z_0}$ . The sign  $+$  is emphasized in this expression as well as in Figure 3a. When  $\beta_0 \rightarrow \Psi(\alpha_0)$ ,  $T_{Z_0Z_0} \rightarrow 0$ . The zero value of the tensor component  $T_{Z_0Z_0}$  is attained, but in this case it does not correspond to a principal component. When  $\beta_0 < \Psi(\alpha_0)$ , the  $B_0$  direction does not intersect the hyperbola presented in Figure 3a. However, one can use the complementary quadric, whose equation in the PAS is

$$T_{XX}X^2 + T_{YY}Y^2 - |T_{ZZ}|Z^2 = -1 \quad (2.27)$$

Equation 2.27 corresponds to an elliptical hyperboloid of two sheets (which is not necessarily of revolution) (Figure 3b). The intersection of this hyperboloid by the  $X'(\alpha_0)Z$  plane corresponds to a hyperbola, of which the equation in  $X'(\alpha_0)Z$  is

$$-(\cos^2 \alpha_0 T_{XX} + \sin^2 \alpha_0 T_{YY})X'^2 + |T_{ZZ}|Z^2 = 1 \quad (2.28)$$

Assuming that  $\beta_0 < \Psi(\alpha_0)$ , and using eq 2.28, the intersection radius  $r$  is then given by  $r^{-2} = -\cos^2 \alpha_0 \sin^2 \beta_0 T_{XX} - \sin^2 \alpha_0 \sin^2 \beta_0 T_{YY} + \cos^2 \beta_0 |T_{ZZ}|$ . It follows that  $-r^{-2} = T_{Z_0Z_0}$ . Again, the sign  $-$  is emphasized in this expression as well as in Figure 3b. The relation between  $r^{-2}$  and  $T_{Z_0Z_0}$  is now different but remains easy to visualize. When  $\beta_0 = 0$ ,  $-r^{-2} = -|T_{ZZ}| = T_{ZZ}$ , and the negative principal component is attained.

It has thus been shown that second-rank properties including negative principal components could be represented by a set of two complementary hyperboloids, avoiding the use of ovaloids. Every set of  $T_{ii}$  values (including positive and/or negative and/or zero principal components) can be represented by a quadric (see Figure 4). When two principal components are equal, the

quadrics become surfaces of revolution (the axis of revolution corresponds to the  $T_{ZZ}$  principal component). When  $T_{ii} = T_{\text{iso}}$  (for  $i = X, Y, Z$ ), the quadric is a sphere of radius  $(T_{\text{iso}})^{-1/2}$ . When  $T_{\text{iso}} = 0$ , the radius of the sphere becomes infinite, and this highly degenerate quadric can be represented by a unique point. It will be seen below that these generalized quadrics are suitable not only for the direct representation of anisotropy in solid-state NMR but also for the pictorial representation of MAS, VAS, and so on. Before considering the effects of macroscopic sample reorientations, we illustrate two static experiments by using quadrics, that is, static NMR in the presence of rapid molecular reorientation and 2D correlation experiment involving CSA and dipolar coupling. The use of quadrics exhibiting negative principal components will be emphasized.

**3. Solid-State NMR in the Presence of Molecular Reorientation and 2D Correlations.** First, we illustrate the effect of rapid molecular reorientation on NMR interactions. The heteronuclear dipolar interaction of an isolated  $I-S$  spin pair is considered. Following eq 2.7a, the geometrical part of the dipolar interaction is well described by the tensor

$$\begin{bmatrix} 1 & 0 & 0 \\ 0 & 1 & 0 \\ 0 & 0 & -2 \end{bmatrix}$$

As stated above, this tensor can be represented by a set of two complementary hyperboloids of revolution (as  $\eta_D = 0$ ), whose equations in the dipolar PAS are

$$X^2 + Y^2 - 2Z^2 = \pm 1 \quad (3.1)$$

The  $I-S$  bond direction corresponds to the  $Z$  axis of the PAS and to the axis of revolution of the hyperboloids (Figure 5a). Using eq 2.26,  $tg^2\Psi = 2$  or  $\Psi = \zeta_m$ . One notes that  $\Psi$  is independent of  $\alpha_0$ , as the tensor is axially symmetric. Symbols  $-$  and  $+$  in Figure 5 are referred to  $-r^{-2} = D_{Z_0Z_0}$  and to  $+r^{-2} = D_{Z_0Z_0}$  when  $\beta_0$  varies from  $0^\circ$  to  $90^\circ$ . It is then possible to represent half of the derived Pake doublet corresponding to  $\nu_D = +(D/2)(1 - 3\cos^2\beta_0)$  (see eqs 2.13, 2.14 and Figure 5b). The second branch of the  $I-S$  Pake doublet is obtained by symmetry. For  $\beta_0 = \zeta_m$ ,  $r \rightarrow \infty$  and the zero value of the tensor is attained: the dipolar splitting vanishes when the  $I-S$  spin pair is at the "magic-angle" from the  $B_0$  field.

It was observed for a long time that rapid anisotropic molecular reorientation led to partial averaging of the different interactions.<sup>1,21</sup> We illustrate such averaging by considering averaged hyperboloids, representing the effect of motion. We suppose that the  $I-S$  pair reorients rapidly around a molecular axis  $Z_M$ , which makes the angle  $\chi$  with  $I-S$  (Figure 6a, with  $\chi > \Psi = \zeta_m$ ). The rotation of the associated set of hyperboloids (Figure 5a) around the molecular axis leads to averaged surfaces. These new quadrics are surfaces of revolution, with the molecular axis  $Z_M$  as the new axis of revolution. The averaged principal component  $\overline{D}_{||}$  associated with this axis is given by the intersection of the old quadrics (Figure 5a) by the molecular axis direction  $Z_M$ :

$$\overline{D}_{||} = \frac{1}{(r^2)_\chi} = 1 - 3\cos^2\chi \quad (3.2)$$

$\overline{D}_{||} > 0$  as  $\chi > \Psi = \zeta_m$ . The second averaged principal component  $\overline{D}_{\perp}$  is given by trace invariance, that is  $2\overline{D}_{\perp} + \overline{D}_{||} = 0$ . It follows that

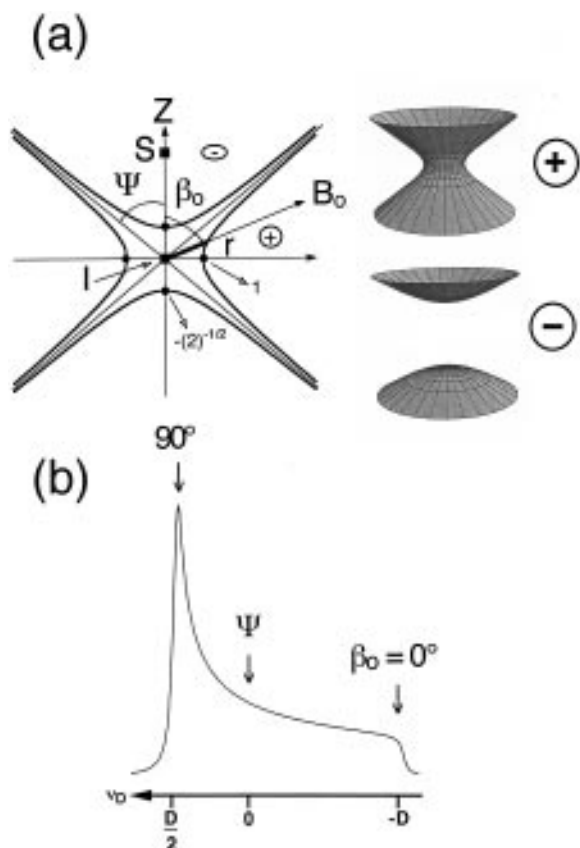


**Figure 5.** Pictorial representation of the heteronuclear dipolar interaction (isolated  $I-S$  spin pair). (a) Set of two hyperboloids of revolution representing the geometric part of the interaction. + and - correspond to the conventions  $+r^{-2} = D_{z_0 z_0}$  and  $-r^{-2} = D_{z_0 z_0}$ . In this case,  $\Psi = \zeta_m$ . (b) Derived powder pattern (one half). For the three orientations of  $B_0$ ,  $\beta_0 = 0^\circ$ ,  $\Psi = \zeta_m$  and  $90^\circ$ , one obtains  $(-r^{-2})_{0^\circ} = -2$ ;  $(+r^{-2})_{\Psi = 0^\circ} = 0$ ;  $(+r^{-2})_{90^\circ} = 1$  and  $(\nu_D)_{\Psi, 90^\circ} = +(D/2)(+r^{-2})_{\Psi, 90^\circ}$ ;  $(\nu_D)_{0^\circ} = +(D/2)(-r^{-2})_{0^\circ}$ ; with  $D = (\mu_0/4\pi)(\hbar/2\pi)(\gamma_I \gamma_S/r_{I-S}^3)$  (see eq 2.7b).

$$\overline{D}_\perp = \frac{3 \cos^2 \chi - 1}{2} \quad (3.3)$$

$\overline{D}_\perp < 0$ . In the new frame (with  $Z_M$  as the unique axis), the equations of the new averaged quadrics representing the rapid reorientation of the  $I-S$  spin pair are given by

$$\frac{3 \cos^2 \chi - 1}{2} (X_M^2 + Y_M^2) + (1 - 3 \cos^2 \chi) Z_M^2 = 1 \quad (3.4)$$

$$\frac{3 \cos^2 \chi - 1}{2} (X_M^2 + Y_M^2) + (1 - 3 \cos^2 \chi) Z_M^2 = -1 \quad (3.5)$$

These equations correspond to a hyperboloid of revolution of two sheets (eq 3.4) and to a hyperboloid of revolution of one sheet (eq 3.5). The hyperboloid of two sheets is characterized by  $\mathbf{H}$  (see Figure 6b), which is directly related to  $\overline{D}_\perp$ . As  $\overline{D}_\perp > 0$ , the sign + is added to the hyperboloid of two sheets. As stated above, it corresponds to the relation  $+r^{-2} = D_{z_0 z_0}$ . The sign - is therefore added to the hyperboloid of one sheet and corresponds to the relation  $-r^{-2} = D_{z_0 z_0}$ . One can then deduce half of the corresponding Pake doublet (Figure 6c). Comparing Figures 5b and 6c, it is thus shown that the overall anisotropy is modulated under fast reorientation by the factor  $(3 \cos^2 \chi - 1)/2$ . This result is general for axially symmetric second-rank tensors.<sup>1</sup> When  $\chi \rightarrow \Psi = \zeta_m$ ,  $\mathbf{G} \rightarrow \infty$  and  $\mathbf{H} \rightarrow \infty$  (Figure 6b).  $r^{-2} \rightarrow 0$  for every orientation of  $B_0$  from  $Z_M$ , and the anisotropy

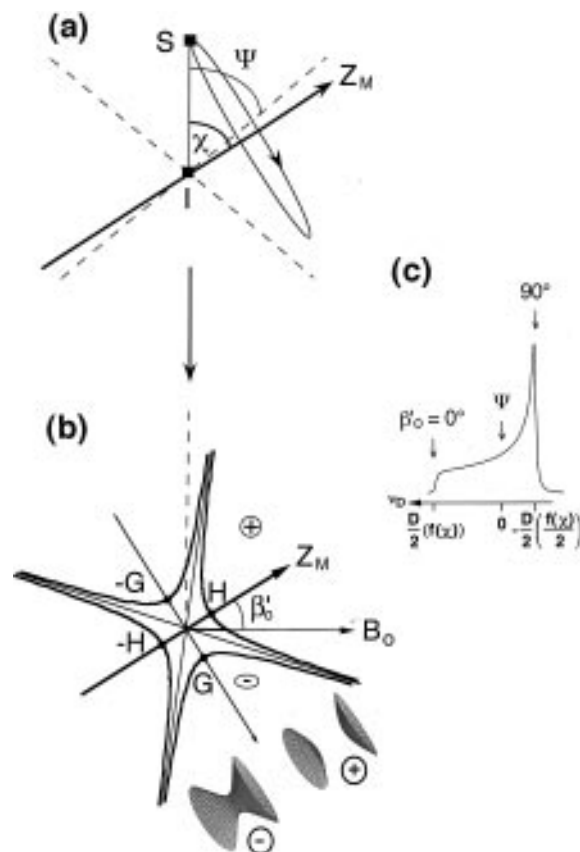


**Figure 6.** Representation of anisotropic motional averaging of the heteronuclear dipolar interaction (isolated spin pair). (a) Fast reorientation of the  $I-S$  pair around the molecular axis  $Z_M$  ( $\chi > \Psi = \zeta_m$ ). (b) Averaged hyperboloids of revolution.  $\mathbf{G} = ((1 - 3 \cos^2 \chi)/2)^{-1/2}$ ;  $\mathbf{H} = (1 - 3 \cos^2 \chi)^{-1/2}$ . (c) Derived powder pattern (one half). For the three orientations of  $B_0$ ,  $\beta'_0 = 0^\circ$ ,  $\Psi = \zeta_m$  and  $90^\circ$ , one obtains  $(+r^{-2})_{0^\circ} = 1 - 3 \cos^2 \chi$ ;  $(+r^{-2})_{\Psi = 0^\circ} = 0$ ;  $(-r^{-2})_{90^\circ} = -(1 - 3 \cos^2 \chi)/2$  and  $(\nu_D)_{0^\circ, \Psi} = +(D/2)(+r^{-2})_{0^\circ, \Psi}$ ;  $(\nu_D)_{90^\circ} = +(D/2)(-r^{-2})_{90^\circ}$ ;  $D$  as in Figure 5;  $f(\chi) = 1 - 3 \cos^2 \chi$ .

due to the dipolar coupling vanishes. The case  $\chi < \Psi$  can be treated as stated above. When  $\chi = 0$ , the “static” quadrics (Figure 5a) are not affected by the reorientation (as they are of revolution) and no modulation of the anisotropy is observed. The same approach can be applied to all quadrics presented in Figure 4. It should also be noted that the representation using sets of averaged hyperboloids can be applied to quadrupolar nuclei with  $I = 1$ . Indeed, the formalism is similar, as shown by eqs 2.7a, 2.8, and 2.18.

Now, we illustrate with quadrics “CSA/dipolar” correlation experiments. Several pulse sequences have been designed for the direct correlation of dipolar interaction and chemical shift in static 2D NMR experiments.<sup>22,23</sup> Other sequences are also devoted to the correlation of tensorial quantities, such as 2D exchange experiments.<sup>24,25</sup> We consider a unique isolated  $I-S$  spin pair and assume that the associated chemical shift tensor (for  $I$ ) is axially symmetric (with  $\sigma_{XX}$  and  $\sigma_{YY} = \sigma_\perp > 0$  and  $\sigma_{ZZ} = \sigma_\parallel > 0$ ). We assume moreover that the two PASs are coincident. In this case, the relevant quadrics in the unique PAS are

$$\sigma_\perp (X^2 + Y^2) + \sigma_\parallel Z^2 = 1 \quad (3.6)$$

$$X^2 + Y^2 - 2Z^2 = \pm 1 \quad (3.7)$$

Equation 3.6 corresponds to an ellipsoid of revolution. Equations 3.7, which are related to the geometrical part of the dipolar

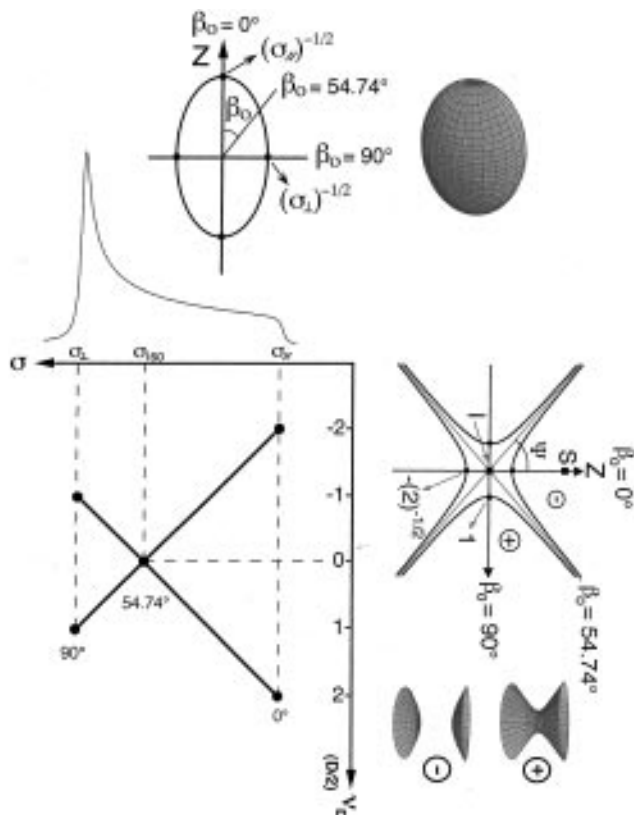


**Figure 7.** Pictorial representation of a 2D “CSA/dipolar” correlation experiment. Three sets  $\{(r^{-2})_{\sigma}, (r^{-2})_{\text{D}}\}$  corresponding to  $\beta_0 = 0^\circ$ ,  $\zeta_m$ , and  $90^\circ$  are represented.

interaction, correspond to the set of complementary hyperboloids of revolution presented above. For one particular crystallite, the intersection  $(r)_{\sigma}$  of the ellipsoid in the  $B_0$  direction gives the resonance on the second dimension (shielding dimension), whereas the intersection  $(r)_{\text{D}}$  of the hyperboloids gives the dipolar splitting on the first dimension (dipolar dimension). In Figure 7, three particular orientations of  $B_0$  are represented. For  $\beta_0 = 0^\circ$ ,  $(r^{-2})_{\sigma} = \sigma_{\parallel}$  is associated with the maximum dipolar splitting as  $(r)_{\text{D}}$  is minimum. Indeed,  $(r)_{\text{D}} = 2^{-1/2}$  or  $(r^{-2})_{\text{D}} = 2$ . Using eq 2.13, 2.14, and  $(-r^{-2})_{\text{D}} = T_{Z_0 Z_0}$ , one obtains  $\nu_{\text{D}} = \pm D$ . For  $\beta_0 = \zeta_m$ ,  $(r^{-2})_{\sigma} = (2\sigma_{\perp} + \sigma_{\parallel})/3 = \sigma_{\text{iso}}$  is associated with a vanishing dipolar splitting ( $(r)_{\text{D}} \rightarrow \infty$  as  $\beta_0 \rightarrow \Psi = \zeta_m$ ). Finally, for  $\beta_0 = 90^\circ$ ,  $(r^{-2})_{\sigma} = \sigma_{\perp}$  is associated with a nonzero dipolar splitting (half of the maximum splitting observed for  $\beta_0 = 0^\circ$ ). The “scissors” pattern shown in Figure 7 has been previously observed in the case of a  $^{13}\text{C}$  cross polarization (CP) NMR experiment on powdered ferrocene  $\text{Fe}(\eta\text{-C}_5\text{H}_5)_2$ .<sup>23</sup> It has thus been shown that the dominant ridges of 2D static spectra could be easily illustrated by using quadrics. The generalization to noncoincident tensors is easily achieved by transposing the hyperboloid equations into the CSA PAS. We now turn to the pictorial representation of macroscopic reorientations of powdered samples, that is, MAS, MAH, VAS, and SAS.

#### 4. Magic-Angle Spinning

Andrew and Lowe<sup>10,11</sup> realized that rapid macroscopic rotation of samples at the “magic-angle” ( $\theta = \zeta_m$ ) led to the suppression of anisotropic first-order interactions.  $\theta$  corresponds to the angle between the rotor axis and  $B_0$ . MAS is one of the most used solid-state NMR techniques, as it allows the obtainment of high-resolution spectra. The mathematical treatment of MAS is generally done by using spherical components of the involved

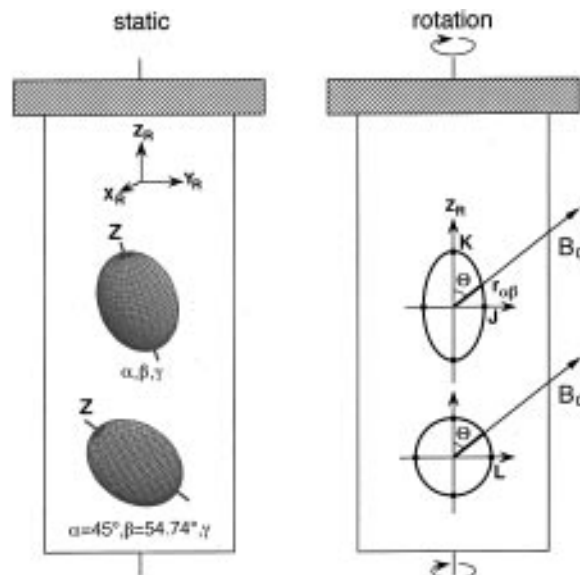


**Figure 8.** Pictorial representation of magic-angle spinning (MAS). We assume that  $T_{ii} > 0$  for  $i = X, Y, Z$ . In the static rotor (left side), the crystallites are randomly oriented from the  $(X_{\text{R}}Y_{\text{R}}Z_{\text{R}})$  rotor frame. The ellipsoids are drawn in the PAS of each crystallite (only the  $Z$  axes are represented). The Euler angles  $(\alpha, \beta, \gamma)$  (see Figure 1) connect the PAS and  $(X_{\text{R}}Y_{\text{R}}Z_{\text{R}})$ . In the rapidly rotating rotor (right side), the corresponding averaged ellipsoids are represented. They are of revolution, and they all admit  $Z_{\text{R}}$  as the unique axis of revolution. When  $\alpha = 45^\circ$  and  $\beta = \zeta_m$ , a sphere is obtained.  $\mathbf{J} = (T_{\perp})^{-1/2}$  (see eq 4.3);  $\mathbf{K} = (T_{\parallel})^{-1/2}$  (see eq 4.4);  $\mathbf{L} = (T_{\text{iso}})^{-1/2}$ .

tensors and Wigner rotation operators.<sup>1</sup> It is then shown that Hamiltonians can be written as the sum of isotropic parts (involving traces of the different tensors) and anisotropic parts containing  $1/2(3\cos^2 \theta - 1)$  as a prefactor. When  $\theta = \zeta_m$ , anisotropic effects on the line shapes vanish. We shall illustrate the effects of MAS by considering Cartesian tensors (or  $3 \times 3$  matrices) and simple frame transformations. Let us consider an interaction represented by a symmetrical second-rank tensor with  $T_{ii} > 0$  in the corresponding PAS. We consider a rotor-fixed frame  $(X_{\text{R}}Y_{\text{R}}Z_{\text{R}})$ , which is oriented by the Euler angles  $(\alpha, \beta, \gamma)$  from the PAS (Figure 8). The expression of  $[\mathbf{T}]_{(X_{\text{R}}Y_{\text{R}}Z_{\text{R}})}$  is given by

$$[\mathbf{T}]_{(X_{\text{R}}Y_{\text{R}}Z_{\text{R}})} = P^{-1}(\alpha, \beta, \gamma)[\mathbf{T}]_{\text{PAS}} P(\alpha, \beta, \gamma) \quad (4.1)$$

The matrix  $P$  and matrix elements  $T_{i_{\text{R}}j_{\text{R}}}$  are given in the Appendix. Spinning the sample around the rotor axis implies that  $\gamma$  becomes a function of  $\omega_{\text{rot}} t$ , where  $\omega_{\text{rot}} = 2\pi\nu_{\text{rot}}$  corresponds to the pulsation of the rotor. We suppose that  $\nu_{\text{rot}} = \infty$ ; that is,  $\nu_{\text{rot}}$  is much higher than the considered interaction in hertz. In this case, averaged values for  $a^2, b^2, \dots, \bar{f}_i$  (see the Appendix) are obtained by considering the following integrals:

$$I_n = \frac{1}{2\pi} \int_0^{2\pi} (\cos \gamma)^{2-n} (\sin \gamma)^n d\gamma \quad (4.2)$$

$I_0 = I_2 = 1/2$  and  $I_1 = 0$ . In  $(X_{\text{R}}Y_{\text{R}}Z_{\text{R}})$ , the averaged expression for  $\mathbf{T}$  under rapid rotation is given by

$$[\bar{\mathbf{T}}]_{(X_{\text{R}}Y_{\text{R}}Z_{\text{R}})} = \begin{bmatrix} \bar{T}_{\perp} & 0 & 0 \\ 0 & \bar{T}_{\perp} & 0 \\ 0 & 0 & \bar{T}_{\parallel} \end{bmatrix}_{(X_{\text{R}}Y_{\text{R}}Z_{\text{R}})}$$

with

$$\overline{T}_{\perp} = \frac{1}{2}[(\cos^2 \alpha \cos^2 \beta + \sin^2 \alpha)T_{XX} + (\sin^2 \alpha \cos^2 \beta + \cos^2 \alpha)T_{YY} + \sin^2 \beta T_{ZZ}] \quad (4.3)$$

$$\overline{T}_{\parallel} = \cos^2 \alpha \sin^2 \beta T_{XX} + \sin^2 \alpha \sin^2 \beta T_{YY} + \cos^2 \beta T_{ZZ} \quad (4.4)$$

One notes that  $2\overline{T}_{\perp} + \overline{T}_{\parallel} = 3T_{\text{iso}}$ .  $[\mathbf{T}]_{(X_R Y_R Z_R)}$  is diagonal and corresponds to an ellipsoid of revolution in  $(X_R Y_R Z_R)$ , with  $Z_R$  as the axis of revolution. It should be noted that the  $\overline{T}_{\perp}$  and  $\overline{T}_{\parallel}$  expressions can be easily derived without any calculation. Before the sample reorientation, the intersection  $R$  of the initial quadric in the  $Z_R$  direction (i.e. the rotor axis direction) is given by

$$\frac{1}{R^2} = \cos^2 \alpha \sin^2 \beta T_{XX} + \sin^2 \alpha \sin^2 \beta T_{YY} + \cos^2 \beta T_{ZZ} \quad (4.5)$$

It follows that  $1/R^2 = \overline{T}_{\parallel}$ . The expression  $\overline{T}_{\perp}$  is obtained by trace invariance. This approach is strictly analogous to that used in section 3 for the representation of rapid local reorientation of molecules (see also eqs 3.2 and 3.3). The semiaxes of the averaged quadrics are given by  $(\overline{T}_{\perp})^{-1/2}$  and  $(\overline{T}_{\parallel})^{-1/2}$  (Figure 8). The equation in  $(X_R Y_R Z_R)$  is then

$$\overline{T}_{\perp}(X_R^2 + Y_R^2) + \overline{T}_{\parallel}Z_R^2 = 1 \quad (4.6)$$

It is interesting to note that these quadrics are all different, as  $\overline{T}_{\perp}$  and  $\overline{T}_{\parallel}$  depend explicitly on the Euler angles  $(\alpha, \beta)$  orienting the PAS of a given crystallite and  $(X_R Y_R Z_R)$ . One notes further that if  $\alpha = 45^\circ$  and  $\beta = \zeta_m$ , then  $\overline{T}_{\perp} = \overline{T}_{\parallel} = (T_{XX} + T_{YY} + T_{ZZ})/3 = T_{\text{iso}}$ . The ellipsoid of revolution becomes a sphere of radius  $(T_{\text{iso}})^{-1/2}$  (Figure 8). The intersection  $r_{\alpha\beta}$  of every averaged ellipsoid in the  $B_0$  direction gives the resonance frequency  $T_{\alpha\beta}$  of each crystallite under rotation. Using eq 4.6,

$$\frac{1}{r_{\alpha\beta}^2} = T_{\alpha\beta} = \overline{T}_{\perp} \sin^2 \theta + \overline{T}_{\parallel} \cos^2 \theta \quad (4.7)$$

$\theta$  corresponds to the macroscopic angle between the rotor axis  $Z_R$  and  $B_0$ . Generally,  $T_{\alpha\beta}$  is a function of the initial Euler angles  $(\alpha, \beta)$  (see section 6). However, when  $\theta = \zeta_m$ , eq 4.7 becomes  $r_{\alpha\beta}^{-2} = T_{\alpha\beta} = (2\overline{T}_{\perp} + \overline{T}_{\parallel})/3 = T_{\text{iso}}$ .  $r_{\alpha\beta}$  and  $T_{\alpha\beta}$  are now independent of  $(\alpha, \beta)$ , and one unique resonance frequency is obtained for all crystallites: high-resolution is obtained. This corresponds to a direct pictorial representation of MAS effects on first-order interactions. Another example is given in Figure 9. The geometrical part of the heteronuclear dipolar interaction ( $I-S$  spin pair) is considered. Sets of hyperboloids of revolution are considered (see section 3).  $\beta$  is the relevant angle. In  $(X_R Y_R Z_R)$ , averaged quadrics obtained under rapid rotation are given by

$$\frac{1}{2}(3 \cos^2 \beta - 1)(X_R^2 + Y_R^2) + (1 - 3 \cos^2 \beta)Z_R^2 = \pm 1 \quad (4.8)$$

Sets of hyperboloids for  $\beta > \Psi$  and  $\beta < \Psi$  are shown in Figure 9. All these hyperboloids are different, depending explicitly on  $\beta$  (see the expressions of  $\mathbf{M} \rightarrow \mathbf{Q}$  in Figure 9). However, the angle  $\Phi$  between  $Z_R$  and each asymptote of the averaged quadrics is independent of the initial orientation of any given crystallite. One shows easily (using eq 4.8) that  $\tan^2 \Phi = |(1 -$

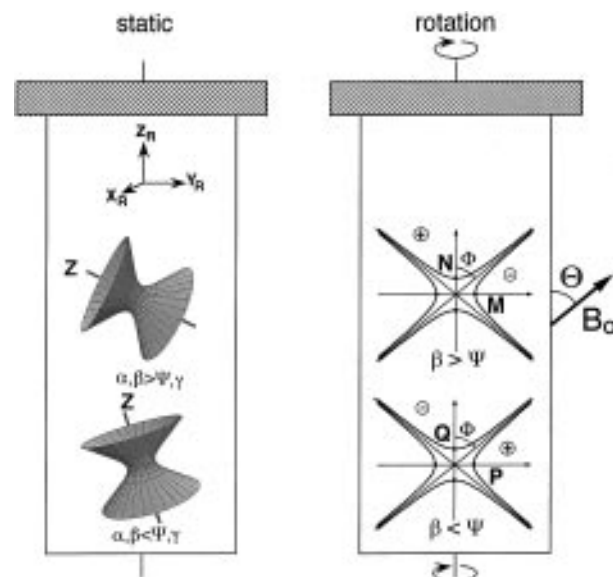


**Figure 9.** Pictorial representation of MAS in the case of the heteronuclear dipolar interaction ( $T_{XX} = T_{YY} > 0, T_{ZZ} < 0$ ). In the static rotor (left side), the crystallites are randomly oriented from the  $(X_R Y_R Z_R)$  rotor frame. The hyperboloids are drawn in the PAS of each crystallite (only the  $Z$  axes are represented). The Euler angles  $(\alpha, \beta, \gamma)$  (see Figure 1) connect the PAS and  $(X_R Y_R Z_R)$ . In the rapidly rotating rotor (right side), the corresponding averaged hyperboloids are represented. One notes that  $\Phi = \zeta_m$ .  $\mathbf{M} = ((1 - 3 \cos^2 \beta)/2)^{-1/2}$ ;  $\mathbf{N} = (1 - 3 \cos^2 \beta)^{-1/2}$ ;  $\mathbf{P} = ((3 \cos^2 \beta - 1)/2)^{-1/2}$ ;  $\mathbf{Q} = (3 \cos^2 \beta - 1)^{-1/2}$ .

$3 \cos^2 \beta)/(1/2)(3 \cos^2 \beta - 1)] = 2$  or  $\Phi = \zeta_m$ . It follows that when  $\theta = \zeta_m$  ( $=\Phi$ ),  $r_{\beta}^{-2} = 0$  for every  $\beta$  value. The isotropic value of the heteronuclear dipolar coupling is attained and the anisotropy vanishes as well under rapid MAS. When  $\beta = \Psi = \zeta_m$ , the semiaxes of the averaged quadrics diverge. They are therefore represented by a point, which corresponds to the zero value of the interaction (see sections 2 and 3). Pictorial representation of MAS was thus presented, avoiding spherical components of the different tensors. Such an approach can be applied to all the quadrics presented in Figure 4 and for every set of  $T_{ii}$  components.

## 5. Magic-Angle Hopping

Bax and co-workers<sup>18</sup> demonstrated that continuous rotation of the sample around an axis at the “magic-angle” is not necessary to obtain isotropic values of interactions in a 2D experiment. Equal evolutions of magnetization for three discrete positions of the rotor (at the “magic-angle” from  $B_0$ ) instead of continuous rotation are sufficient. The pictorial representation of MAS presented above implies averaging of quadrics by continuous rotation. This led to averaged values of  $a^2, b^2, \dots, \bar{f}_i$  (see Appendix) using integrals  $I_n$  (eq 4.2). If the same averaging procedure is possible by discrete regular  $p$  “hops” of the rotor, then one must fulfill the following equations:

$$\frac{1}{2\pi} \int_0^{2\pi} (\cos \gamma)^{2-n} (\sin \gamma)^n d\gamma = \frac{1}{p} \sum_{q=0}^{p-1} \left[ \cos \left( \gamma + \frac{360}{p} \right) \right]^{2-n} \left[ \sin \left( \gamma + \frac{360}{p} \right) \right]^n \quad (5.1)$$

for  $n = 0, 1, 2$  and every  $\gamma$ . Basic trigonometric calculations show that  $p = 3$  corresponds to the minimum number of “hops” (Figure 10) and



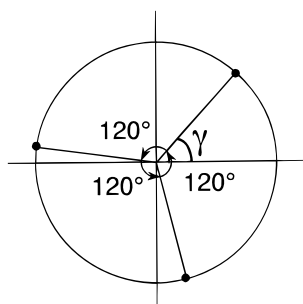


**Figure 10.** Pictorial representation of three regular hops of the rotor during a magic-angle hopping (MAH) experiment. Increments of  $\gamma$  are  $120^\circ$ .

$$\frac{1}{3}[\cos^2 \gamma + \cos^2(\gamma + 120^\circ) + \cos^2(\gamma + 240^\circ)] = \frac{1}{2} = I_0$$

$$\frac{1}{3}[\cos \gamma \sin \gamma + \cos(\gamma + 120^\circ) \sin(\gamma + 120^\circ) + \cos(\gamma + 240^\circ) \sin(\gamma + 240^\circ)] = 0 = I_1$$

$$\frac{1}{3}[\sin^2 \gamma + \sin^2(\gamma + 120^\circ) + \sin^2(\gamma + 240^\circ)] = \frac{1}{2} = I_2 \quad (5.2)$$

This is a direct representation of a MAH experiment. Recently, novel schemes involving ultraslow rotation of the samples were proposed in the literature and referred to as MAT or magic-angle turning.<sup>26</sup> Equations 5.1 and 5.2 can be easily generalized to every  $(\cos \gamma)^r (\sin \gamma)^s$  trigonometric function (with fixed  $t = (r + s)$ ). If one wants to “average” such a function, classic trigonometric calculations show that  $t + 1$  regular hops of the rotor are sufficient. In other words,

$$\frac{1}{2\pi} \int_0^{2\pi} (\cos \gamma)^r (\sin \gamma)^s d\gamma = \frac{1}{t+1} \sum_{q=0}^t \left[ \cos \left( \gamma + q \frac{360}{t+1} \right) \right]^r \left[ \sin \left( \gamma + q \frac{360}{t+1} \right) \right]^s \quad (5.3)$$

for fixed  $t$  and every  $\gamma$ . In this case, the figure obtained after the successive hops is no longer an equilateral triangle ( $t = 2$ , see Figure 10) but a regular polygon of  $t + 1$  vertices. Equation 5.3 will be of particular interest for the direct representation of DAH or dynamic-angle hopping,<sup>27</sup> involving higher-order interactions (such as second-order quadrupolar interaction).

## 6. Variable-Angle Spinning

When  $\theta \neq \zeta_m$ , rapid reorientation of the sample corresponds to VAS. The effects of VAS are easily understood by using the expression of  $T_{\alpha\beta}$  given in eq 4.7. The modulation of the static line width is obtained by variations of  $\alpha$  and  $\beta$ . An example is shown in Figure 11 with  $T_{XX} = T_{YY} = 2$ , and  $T_{ZZ} = 1$  ( $T_{\text{iso}} = 5/3$ ) in arbitrary units. The static line width is given by an ellipsoid of revolution. Under VAS and using eq 4.7,

$$T_{\alpha\beta} \equiv T_\beta = \frac{1}{2}(3 + \cos^2 \beta) \sin^2 \theta + (2 - \cos^2 \beta) \cos^2 \theta \quad (6.1)$$

Moreover, the static line width is given by eq 2.10 with  $\beta_0$  corresponding to the Euler angle between  $B_0$  and the unique  $Z$  axis of the PAS in the static sample:

$$T_{Z_0Z_0} = 2 - \cos^2 \beta_0 \quad (6.2)$$

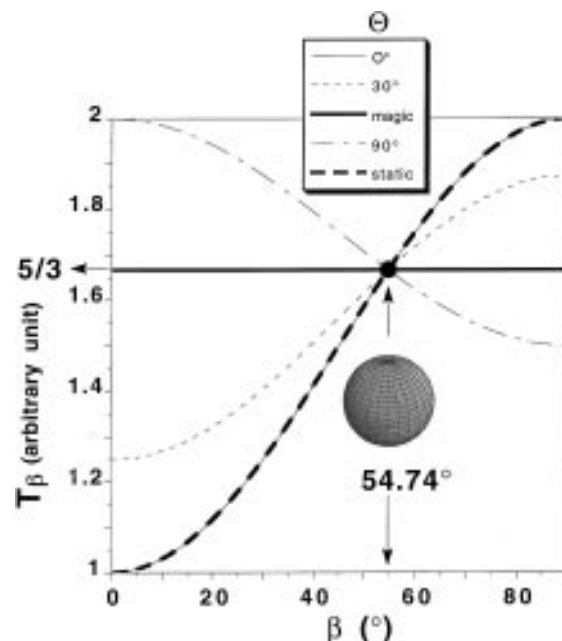


**Figure 11.** Pictorial representation of variable-angle spinning (VAS) for  $T_{XX} = T_{YY} = 2$ , and  $T_{ZZ} = 1$  (au).  $\beta$  is defined as in section 4 and in Figure 8.  $\theta$  corresponds to the angle between  $B_0$  and the rotor. For  $\beta = \zeta_m$ , the averaged quadric corresponds to a sphere of radius  $(T_{\text{iso}})^{-1/2}$ : the intersection radius of this sphere in the  $B_0$  direction is independent of  $\theta$  and corresponds to  $T_{\text{iso}}$ .

For fixed  $\theta$ , the line width under rapid rotation of the sample is then given by  $(T_\beta)_{\text{max}}$  and  $(T_\beta)_{\text{min}}$ . Most of the results of VAS are illustrated in Figure 11.

For  $\theta = 0^\circ$ , no modulation of the static line width is observed. In this case,  $\beta = \beta_0$  and eqs 6.1 and 6.2 are strictly identical.

For  $\theta = \zeta_m$ , a unique resonance at  $T_{\text{iso}} = 5/3$  is observed, as expected from MAS results (section 4).

Derivation of eq 6.1 gives  $(T_\beta)_{\text{max}} = (3 + \cos^2 \theta)/2$  and  $(T_\beta)_{\text{min}} = (2 - \cos^2 \theta)$  for  $\theta < \zeta_m$  and  $(T_\beta)_{\text{max}} = (2 - \cos^2 \theta)$  and  $(T_\beta)_{\text{min}} = (3 + \cos^2 \theta)/2$  for  $\theta > \zeta_m$ . In other words, the static linewidth is modulated by the factor  $(3 \cos^2 \theta - 1)/2$  under rapid VAS at  $\theta$ . This is a general result of the VAS experiment.<sup>19</sup>

As shown in Figure 11, all curves obtained for variable  $\theta$  intersect for  $\beta = \zeta_m$ . In the static sample, the corresponding crystallites are at the “magic-angle” from the rotor axis. Under rapid reorientation of the rotor, the corresponding averaged quadric is a sphere of radius  $(T_{\text{iso}})^{-1/2} = (5/3)^{-1/2}$  (see section 4 and Figure 8). The intersection of this sphere by  $B_0$  at  $\theta$  is evidently independent of  $\theta$  and  $T_{\zeta_m} = T_{\text{iso}}$  (see eq 6.1 for  $\beta = \zeta_m$ ). If  $T_{\text{iso}} = 0$  (as for the dipolar interaction), the averaged sphere is at best represented by a point.

## 7. Miscellaneous

Finally, we illustrate with quadrics the rotation of samples around two different axes (for  $I = 1/2$ ) and wonder about the pictorial representation of higher-rank interactions (for instance, the second-order quadrupolar interaction for  $I = n/2$  with  $n = 3, 5, 7, 9$ ).

The rotation around two axes ( $I = 1/2$ ) (known as SAS or switching-angle spinning) was first introduced by Bax and co-workers<sup>28</sup> in the frame of CP NMR. Indeed, at very high speed MAS, the dipolar interaction that is responsible for the CP transfer of magnetization between the abundant spin bath (for instance  $^1\text{H}$ ) and the much less abundant nuclei (for instance  $^{13}\text{C}$ ) is strongly affected by the rotation of the rotor and even

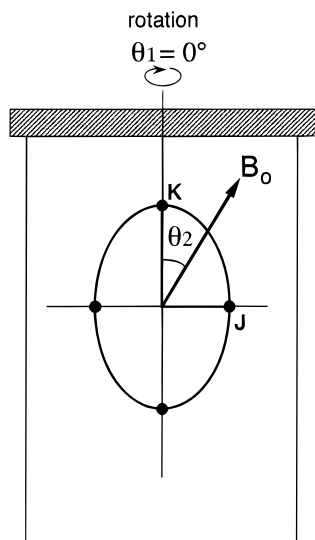


**Figure 12.** Pictorial representation of switching-angle spinning (SAS). The rotor is rapidly rotated at  $\theta_1 = 0^\circ$  (during  $t$ ) and  $\theta_2$  (during  $(1-t)$ ) from  $B_0$  (see text, section 7). **J** and **K** are given in Figure 8.

vanishes. But, as stated above in section 6, NMR interactions are not modulated by the macroscopic rotation if  $\theta = 0^\circ$  (even at infinite rotation speed). The SAS methodology consists of the building up of the  $^{13}\text{C}$  magnetization under CP at  $\theta = 0^\circ$  (at least theoretically) and the detection of signals under high-resolution conditions (i.e.  $\theta = \zeta_m$ ). Zero-angle spinning followed by MAS acquisition was also used for RF-driven spin diffusion experiment.<sup>29</sup> Recently, the SAS technique was applied to complex silicate systems in order to obtain CSA data in poorly resolved lines (by using the  $90^\circ - \zeta_m$  angles pair).<sup>30</sup> In all cases, the acquisition of the spectra occurs at the “magic-angle”, yielding high resolution in the  $F_2$  dimension. We now show that high-resolution spectra may be obtained without rotation at the “magic-angle”. We consider a quadric with  $T_{ii} > 0$ . Under rapid rotation, averaged quadrics are given by eqs 4.3, 4.4, and 4.6. They correspond to ellipsoids of revolution. Rotation of the rotor at  $\theta_1$  and  $\theta_2$  corresponds to the intersections of the averaged quadrics by  $B_0$  at  $\theta_1$  and  $\theta_2$  (Figure 12). We impose  $\theta_1 = 0^\circ$ . The evolution of the rotor during  $t$  at  $0^\circ$  is followed by an evolution during  $1-t$  at  $\theta_2$  (with  $0 < t < 1$ ). High resolution is attained if the following equation is fulfilled for every set  $\{\overline{T}_\perp, \overline{T}_\parallel\}$  (see eq 4.7):

$$tT_{\alpha\beta}(0^\circ) + (1-t)T_{\alpha\beta}(\theta_2) = T_{\text{iso}} \quad (7.1)$$

Equation 7.1 is fulfilled for every set  $\{\overline{T}_\perp, \overline{T}_\parallel\}$  when

$$t = \frac{1 - 3 \cos^2 \theta_2}{3(1 - \cos^2 \theta_2)} \quad \text{and} \quad t > 0 \quad (7.2)$$

The graph of  $t$  versus  $\theta_2$  is represented in Figure 13. The condition  $t > 0$  implies  $\theta_2 > \zeta_m$ . Strictly speaking, this experiment could be compared to the 2D-DAS experiment<sup>13,15</sup> which is devoted to the suppression of second-order quadrupolar broadening: after a  $t_1$  evolution at  $\theta_1 = 0^\circ$ , a  $t_2$  evolution at  $\theta = \theta_2$  would follow (after subsequent hopping of the rotation axis between  $0^\circ$  and  $\theta_2$ ). For

$$\frac{t_2}{t_1} = \frac{1-t}{t} = \frac{2}{1 - 3 \cos^2 \theta_2} \quad (7.3)$$

an echo would occur. This echo would be modulated by  $T_{\text{iso}}$

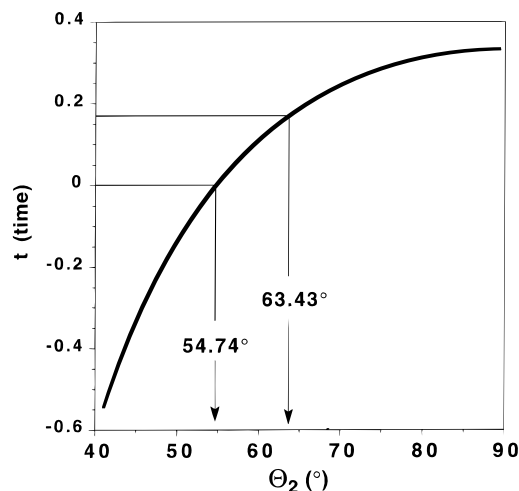


**Figure 13.** Graph of eq 7.2:  $t = (1 - 3 \cos^2 \theta_2) / [3(1 - \cos^2 \theta_2)]$  vs the angle  $\theta_2$ . The first angle  $\theta_1$  is fixed at  $0^\circ$ .

and subsequent double Fourier transformation would lead to a 2D “isotropic/anisotropic” correlation. It should be noted that  $t = 1/6$  implies  $\theta_2 = 63.43^\circ$  (see Figure 13) and  $t_2/t_1 = 5$ . Indeed,  $(0^\circ, 63.43^\circ)$  corresponds to one of the DAS angle pairs. Such an experiment could be interesting for CP experiments involving nuclei with strong CSA (such as very anisotropic  $^{13}\text{C}$  nuclei or “heavy elements” such as  $^{199}\text{Hg}$ ,  $^{119}\text{Sn}$ , and  $^{113}\text{Cd}$ ) and for which the highest rotation speeds are required. The CP transfer would be achieved at  $0^\circ$  (with maximum efficiency) and the detection of signals would occur at  $\theta_2$ . The anisotropic patterns would be then modulated by the factor  $(3 \cos^2 \theta_2 - 1)/2$  in the anisotropic dimension. As the CSAs are large, the choice of  $\theta_2$  in the vicinity of the “magic-angle” would lead to relatively small broadening of the patterns, leading to an important S/N gain. To our knowledge, such an experiment has not been proposed in the literature. Nevertheless, it can be compared to the CP-DAS experiment proposed by Baltisberger and co-workers involving the  $(0^\circ, 63.43^\circ)$  angle pair and devoted to second-order quadrupolar interactions.<sup>31</sup>

For higher-rank interactions (such as the second-order quadrupolar interaction), it is well-known that the energy levels of the central transition of a quadrupolar nucleus with  $I = 3/2, 5/2, 7/2, 9/2$  when perturbed to the second-order are complex fourth-degree trigonometric functions, involving the Euler angles  $(\alpha_0, \beta_0, \gamma_0)$  between the EFG tensor and  $B_0$ .<sup>32</sup> Moreover, sophisticated methods such as DAS,<sup>13</sup> DOR,<sup>14</sup> and MQ-MAS<sup>16</sup> were recently implemented in order to suppress the second-order broadening (the total suppression is actually impossible under simple MAS or even VAS). All these techniques were described by using spherical tensors, Wigner rotation operations, and a careful analysis of the trigonometric expressions in terms of  $P_2(\cos \theta)$  and  $P_4(\cos \theta)$  (where  $P_2$  and  $P_4$  correspond to the second- and fourth-degree Legendre polynomials;  $\theta$  is the angle between the rotor axis and  $B_0$ ). Obviously, the generalized quadrics presented above can not give a satisfactory representation of second-order effects. Indeed, the quadrics led essentially to second-degree trigonometric functions (see eqs 2.21a, 2.21b). However, we will show in a next article that static second-order effects can be well-represented by fourth-degree surfaces (for every value of  $\eta_Q$ ). Moreover, simple Cartesian transformations of these novel surfaces under fast reorientation will allow us to illustrate the effects of MAS, VAS, DAS, DAH, DOR, MQ-MAS, and SAS<sup>33</sup> on the central transition of quadrupolar nuclei. Overtone spectroscopy<sup>34,35</sup> devoted to integer spins (such as  $^{14}\text{N}$ ,  $I = 1$ ) will also be analyzed under static conditions and under

## CHART 1

$$P = \begin{bmatrix} a & d & g \\ b & e & h \\ c & f & i \end{bmatrix} = \begin{bmatrix} (\cos \alpha \cos \beta \cos \gamma - \sin \alpha \sin \gamma) & (-\cos \alpha \cos \beta \sin \gamma - \sin \alpha \cos \gamma) & (\cos \alpha \sin \beta) \\ (\sin \alpha \cos \beta \cos \gamma + \cos \alpha \sin \gamma) & (-\sin \alpha \cos \beta \sin \gamma + \cos \alpha \cos \gamma) & (\sin \alpha \sin \beta) \\ (-\sin \beta \cos \gamma) & (\sin \beta \sin \gamma) & (\cos \beta) \end{bmatrix}$$

fast reorientation of the sample. In all cases, no explicit reference to Legendre polynomials will be made.

## 8. Conclusions

In this paper, we have shown that generalized quadrics can give a satisfactory representation of first-order interactions for every set of principal components. The use of higher-degree surfaces such as ovaloids is not necessary. Moreover, transformation of these Cartesian tensors upon rapid reorientation led to averaged quadrics with known analytical expressions. These averaged quadrics allowed us to represent very simply the effects of MAS, MAH, and VAS on first-order interactions. The effect of SAS was also analyzed. However, the quadrics are not suitable for the representation of second-order interactions. Novel surfaces are required and will be presented in a forthcoming paper.

**Acknowledgment.** The authors are grateful to Dr. P. P. Man for careful reading of the manuscript and for helpful discussions.

## Appendix

The expression of the matrix  $P$  relating two frames oriented by the Euler angles  $(\alpha, \beta, \gamma)$  (defined as in Figure 1) (see section 2) is shown in Chart 1.

The expressions of matrix elements  $T_{iRjR}$ , calculated in the  $(X_R Y_R Z_R)$  frame (see section 4), is

$$[(T_{iRjR})_{(X_R Y_R Z_R)}] = P^{-1}(\alpha, \beta, \gamma) [T]_{PAS} P(\alpha, \beta, \gamma)$$

with

$$T_{1R1R} = a^2 T_{XX} + b^2 T_{YY} + c^2 T_{ZZ}$$

$$T_{2R2R} = d^2 T_{XX} + e^2 T_{YY} + f^2 T_{ZZ}$$

$$T_{3R3R} = g^2 T_{XX} + h^2 T_{YY} + i^2 T_{ZZ}$$

$$T_{1R2R} = ad T_{XX} + be T_{YY} + cf T_{ZZ}$$

$$T_{1R3R} = ag T_{XX} + bh T_{YY} + ci T_{ZZ}$$

$$T_{2R3R} = dg T_{XX} + eh T_{YY} + fi T_{ZZ}$$

$a \rightarrow i$  are given above.

## References and Notes

- (1) Mehring, M. *Principles of High Resolution NMR in Solids*, 2nd ed.; Springer-Verlag: Berlin, 1983; Chapter 2.
- (2) Haeberlen, U. *High Resolution NMR in Solids, Selective Averaging*; Academic Press: New York, 1976; Chapters 3 and 4.
- (3) Bloembergen, N.; Rowland, T. J. *Phys. Rev.* **1955**, *97*, 1679.
- (4) Pake, G. E. *J. Chem. Phys.* **1948**, *16*, 327.
- (5) Pound, R. V. *Phys. Rev.* **1950**, *79*, 685.
- (6) Stauss, G. H. *J. Chem. Phys.* **1964**, *40*, 1988.
- (7) Nye, J. F. *Physical Properties of Crystals*, 2nd ed.; Clarendon Press: Oxford, 1989; Chapter 1.
- (8) Meier, B. *Chimia* **1994**, *48*, 56.
- (9) Radeaglia, R. *Solid State NMR* **1995**, *4*, 317.
- (10) Andrew, E. R.; Bradbury, A.; Eades, R. G. *Nature* **1958**, *182*, 1659.
- (11) Lowe, I. J. *Phys. Rev. Lett.* **1959**, *2*, 285.
- (12) Ganapathy, S.; Schramm, S.; Oldfield, E. *J. Chem. Phys.* **1982**, *77*, 4360.
- (13) Llor, A.; Virlet, J. *Chem. Phys. Lett.* **1988**, *152*, 248.
- (14) Samoson, A.; Lippmaa, E.; Pines, A. *Mol. Phys.* **1988**, *65*, 1013.
- (15) Chmelka, B. F.; Zwanziger, J. W. *Solid State NMR VI: Methods and Applications of Solid State NMR, NMR Basic Principles and Progress*; Springer-Verlag: Berlin, 1994; Vol. 33.
- (16) Frydman, L.; Harwood, J. S. *J. Am. Chem. Soc.* **1995**, *117*, 5367.
- (17) Samoson, A.; Sun, B. Q.; Pines, A. *Pulsed Magnetic Resonance: NMR, ESR and Optics*; Clarendon Press: Oxford, 1992; Chapter 3.
- (18) Bax, A.; Szeverenyi, N. M.; Maciel, G. E. *J. Magn. Reson.* **1983**, *52*, 147.
- (19) Stejskal, E. O.; Schaefer, J.; McKay, R. A. *J. Magn. Reson.* **1977**, *25*, 569.
- (20) Harris, R. K. *Multinuclear Magnetic Resonance in Liquids and Solids—Chemical Applications*; Kluwer Academic: Dordrecht, 1990; Chapter 15.
- (21) Gutowsky, H. S.; Pake, G. E. *J. Chem. Phys.* **1950**, *18*, 162.
- (22) Linder, M.; Höhener, A.; Ernst, R. R. *J. Chem. Phys.* **1980**, *73*, 4959.
- (23) Palmas, P.; Tekely, P.; Canet, D. *J. Magn. Reson. A* **1993**, *104*, 26.
- (24) Hirschinger, J.; Schaefer, D.; Spiess, H. W.; Lovinger, A. J. *Macromolecules* **1991**, *24*, 2428.
- (25) Schmidt-Rohr, K.; Spiess, H. W. *Multidimensional Solid State NMR and Polymers*; Academic Press: London, 1994; Chapter 7.
- (26) Gan, Z. *J. Am. Chem. Soc.* **1992**, *114*, 8307.
- (27) Gann, S. L.; Baltisberger, J. H.; Pines, A. *Chem. Phys. Lett.* **1993**, *210*, 405.
- (28) Bax, A.; Szeverenyi, N. M.; Maciel, G. E. *J. Magn. Reson.* **1983**, *55*, 494.
- (29) Tomaselli, M.; Meier, B. H.; Baldus, M.; Eisenegger, J.; Ernst, R. R. *Chem. Phys. Lett.* **1994**, *225*, 131.
- (30) Zhang, P.; Dunlap, C.; Florian, P.; Grandinetti, P. J.; Farnan, I.; Stebbins, J. F. *J. Non Cryst. Solids* **1996**, *204*, 294.
- (31) Baltisberger, J. H.; Gann, S. L.; Grandinetti, P. J.; Pines, A. *Mol. Phys.* **1994**, *81*, 1109.
- (32) Man, P. P. *Encyclopedia of Nuclear Magnetic Resonance*; Wiley: Chichester, 1996; Vol. 6, p 3838.
- (33) Shore, J. S.; Wang, S. H.; Taylor, R. E.; Bell, A. T.; Pines, A. *J. Chem. Phys.* **1996**, *105*, 9412.
- (34) Tycko, R.; Opella, S. J. *J. Chem. Phys.* **1987**, *86*, 1761.
- (35) Takegoshi, K.; Hikichi, K. *Chem. Phys. Lett.* **1992**, *194*, 359.